2017

Upgrades to and Current Research Efforts Involving the Tow Tank Facility at the Naval Postgraduate School

Klamo, Joseph T.; Jones, Leo M.; Kwon, Young W.; Didoszak, Jarema M.

Society of Petroleum Engineers (SPE)

Klamo, J. T., et al. "Upgrades to and current research efforts involving the tow tank facility at the Naval Postgraduate School." Proceedings of the 30th American Towing Tank Conference. 2017.
https://hdl.handle.net/10945/65779

THE 30th AMERICAN TOWING TANK CONFERENCE
WEST BETHESDA, MARYLAND, OCTOBER 2017

Upgrades to and Current Research Efforts Involving the Tow Tank Facility at the Naval Postgraduate School

Joseph T. Klamo*, Systems Engineering, Naval Postgraduate School, Monterey CA
Leo M. Jones, Undersea Warfare Graduate Student, Naval Postgraduate School, Monterey CA
Young W. Kwon, Mechanical and Aerospace Engineering, Naval Postgraduate School, Monterey CA
Jarema M. Didoszak, Mechanical and Aerospace Engineering, Naval Postgraduate School, Monterey CA
*corresponding author, email: jklamo@nps.edu

ABSTRACT

The Naval Postgraduate School has added wave making capability to the existing small tow tank that resides on campus. A new collaborative research effort between the Systems Engineering and Mechanical and Aerospace Engineering Departments is underway that utilizes this new capability. The aim of this new effort is to understand and predict the unsteady hydrodynamic loads experienced by a submerged vehicle operating near the surface.

The tow tank was originally built around 1970 but only had the capability of testing models at slow speed in calm water. Even with this limited capability, a number of interesting studies were conducted in the facility including measuring the drag on a towed hydropower turbine and examining the forces due to collisions between floating ice-equivalent objects and a composite plate.

The new wave making capability in the tow tank is provided by a vertical plunging wedge that was modeled off of the sediment tank wavemaker at the United States Naval Academy. The wedge rides on a pair of vertical rails with the oscillation amplitude and frequency controlled by a linear actuator and electric motor. A variable angle wave absorbing beach is planned for the opposite end of the tank. An additional component of this modernization effort is the creation of a numeric tow tank, using ANSYS CFX, which can simulate the wave dynamics in the tank. This allows complementary numerical and experimental components of future research efforts.

The current experimental effort involves characterizing the performance of the wavemaker and quantifying the wave environment throughout the tank. The wedge to wave amplitude transfer function has been determined over the relevant amplitude and frequency space. The uniformity of a wave crest has also been examined. For the numeric tow tank work, the wedge motion has been duplicated and the simulated wave elevation and propagation down the tank are being compared to experimentally measured results.

NOTATION

CFD	computational fluid dynamics
EMB	Experimental Model Basin
LDPE	low density polyethylene
NPS	Naval Postgraduate School
a	wave amplitude
a_{w}	wedge amplitude
f	oscillation frequency
H	wave height
k	angular wave number
z	vertical position of the wedge
λ	wavelength
η	wave elevation
ϕ	phase shift
Ψ	wedge-to-wave amplitude transfer function

INTRODUCTION

The U.S. Navy has utilized tow tanks since the inception of its experimental testing efforts. In fact, the Navy's first experimental facility, the Experimental Model Basin (EMB) located at the Washington Navy Yard in Washington DC, consisted of a tow tank. Initially, tow tank testing was indispensable in supporting the development of powering and resistance curves in calm water for surface ships. The applications of tow tank testing have since expanded beyond powering and resistance studies to include, among other things, seakeeping performance in waves for surface ships, stability and control of underwater vehicles, slamming of planing craft, and studies of the wake generated from surface and submerged vessels. The need for experimental results from tow tank testing to support the development of the Navy's future fleet will continue into the foreseeable future even as the power of computers continually increases.

The tow tank at the Naval Postgraduate School (NPS) was originally built around 1970. Due to its rather short length, even by academic standards, the only traditional naval hydrodynamic studies supported by the facility were tests using small models at low forward speeds. The small models and low speeds were required for sufficient run durations to collect data as well as allow for starting and stopping of the model within the length of the tank. To get around this limitation, inventive non-traditional naval hydrodynamics testing, that still had Navy applications, has frequently been undertaken. Some examples of these efforts include studying energy generation from a hydropower turbine and the structural response of composite materials due to impacts with floating objects.

Recently, a joint effort between the Systems Engineering and the Mechanical and Aerospace Engineering departments was undertaken to add a wave making capability to the tow tank. The addition of this new capability was recognized as greatly increasing the usefulness of the tank. The most important aspect of this new capability is that testing in waves without the application of forward motion can be undertaken for both surface ships and underwater vehicles. This capability then serves as the starting point for investigating a large number of interesting and useful traditional Navy hydrodynamics problems involving waves. At the same time, this approach eliminates the major weakness of the tank, namely its short length, since there is no forward speed. This allows larger models to be used and, in principle, infinite run durations. It also allows for the expansion of the previous nontraditonal efforts to be further investigated through the inclusion of wave forces to build off the initial efforts.

Figure 1: Low density polyethylene blocks in the original tow tank as part of a previous research effort.

PREVIOUS WORK

The original tow tank was used for a variety of faculty and graduate student research activities over the years. Sarpkaya & Isaacson (1981) is the compilation of many different early research efforts, many looking at the forces on bluff objects due to oscillatory flows. An alternative energy study was undertaken by Platzer et al. (2011) and Bryan et al. (2013) to look at the feasibility of "energy ships" which would be sailing vessels that created hydrogen and oxygen from electrolysis using electricity produced from a hydropower turbine dragged through the water. The most recent series of investigations explored the fluid-structure interaction of a moving composite plate and freely floating objects. The potential application of this study was for a ship traveling in the arctic region with floating ice blocks. The results of that study will be briefly highlighted below with a more complete discussion in Kwon et al. (2016).

Since the tow tank is not in a temperature controlled environment, actual ice could not be used as it would melt during the test and the data would be inconsistent. A substitute material was selected to represent the ice blocks. Low density polyethylene (LDPE), with a density of 924 kg/m^3 which is close to the density of the sea ice, was chosen. The distribution of LDPE was determined using an areal coverage parameter which was the ratio of the total surface area of LDPE blocks to the water surface area where the LDPE blocks were placed. Figure 1 shows the LDPE blocks inserted in the tow tank. In the figure, the area enclosed by the yellow strings indicates the location where the LDPE blocks were placed and is the value used for the water surface area in the areal coverage ratio.

Because LDPE blocks were freely floating, it was difficult to control the exact locations of all the blocks during testing. Therefore, for a constant areal coverage ratio, a large number of tests were repeated to investigate the random distribution of LDPE blocks on the test results. The results did not show much variability even though the actual distribution of blocks was different for each run.

For each test, a composite plate was pulled the length of the tow tank and the response of the plate as it traveled through the clustered LDPE blocks was measured using a strain gage and force gage. Various steady-state speeds and constant acceleration rates were investigated. In addition, the angle the plate made with the free surface was varied to roughly represent the hull angle of different hullforms. Figure 2 shows how the plate angle was defined. Three different plate angles were considered: 0, +30, and -30 degrees.

In order to investigate the impact of only the LDPE blocks on the composite plate, the first set of tests were conducted without LDPE blocks present. The speed and acceleration

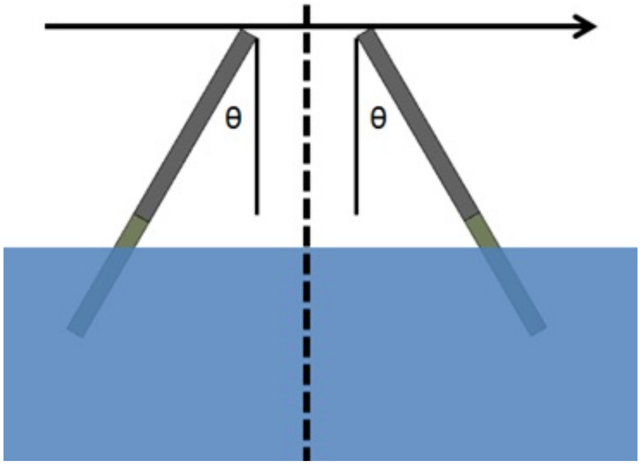

Figure 2: Plate angle definition and convention. The left image is a negative plate angle while the right image shows a positive angle. The black arrow represents the towing direction.

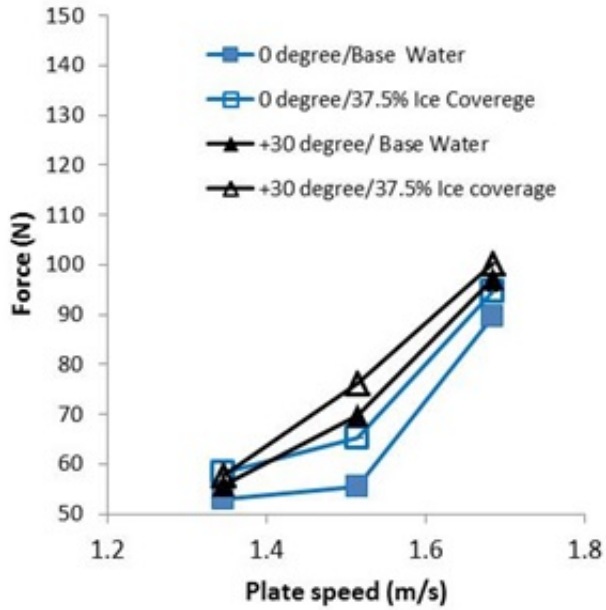

(a) positive and zero plate angles

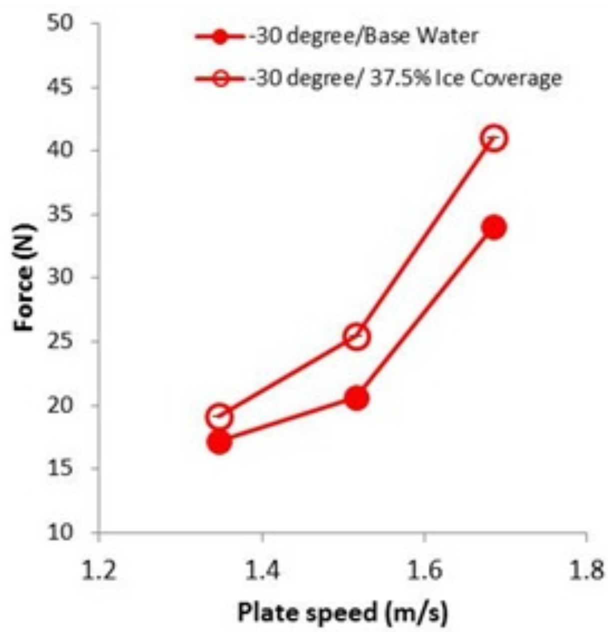

(b) negative plate angle

Figure 3: Drag force as a function of steady-sate towing speed for different plate angles.

rate were varied to establish the baseline data. The drag force and the strain responses of the plate were measured. Then, the same tests were conducted with LDPE blocks inserted into the tow tank. The difference between the two data sets yields the effect of the LDPE blocks. Figure 3 shows the drag force as a function of the steady-state plate speed with different plate angles. Since the negative plate angle produces a much smaller drag force, it is plotted separately. The results show there was an increase in the drag force resulting from the LDPE blocks, which was expected. However, the percentage change is largest for the negative orientation angle. Even though the increase in the drag force is larger with a higher towing speed, the percent change resulting from LDPE blocks is smaller at the higher speed for the negatively angled plate.

An underwater video camera was also attached at the bottom edge of the plate to view the interaction between the plate and the LPDE blocks. The video illustrated that the LDPE blocks moved up the positively orientated plate while they moved down the negatively oriented plate. On the other hand, the LDPE blocks did not move either way for the zero degree plate. A computational fluid dynamics (CFD) analysis showed that the pressure gradient from the water free surface toward the bottom of the plate was different for each orientation angles. Figure 4 compares the pressure gradient for two different orientation angles. The negative orientation angle has pressure decrease along the water depth. That suggests that the LDPE blocks move down the plate. On the other hand, the positive orientation angle shows an initial increase in the pressure along the water depth. This collaborates the observed push-up of the LDPE blocks in front of the plate with the positive orientation angle.

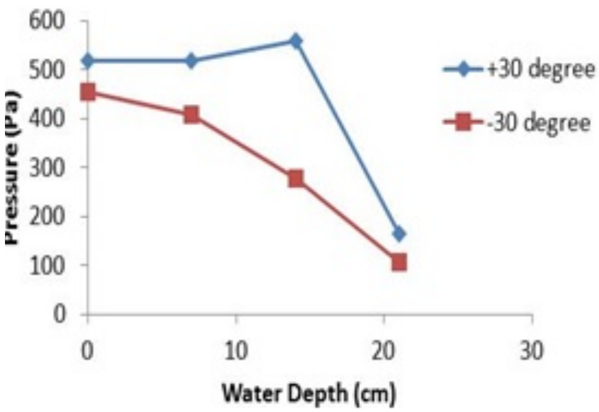

Figure 4: Plot of pressure as a function of water depth in front of the plates with two different plate angles.

DESCRIPTION OF EXPERIMENTAL FACILITY

Tow Tank

The NPS tow tank was originally constructed in the 1970s and is located in the Hydrodynamics Laboratory in Halligan Hall. The tow tank, shown in Figure 5 is 0.914 meters (3 feet) wide by 1.219 meters (4 feet) deep and has a length of 10.973 meters (36 feet). It is constructed of aluminum and is support by two steel I-beams at the bottom. One side of the tank is lined with Plexiglass observation panels for mostly unobstructed flow visualization access, while the far side is solid aluminum plate. The tank is filled with freshwater and has a maximum capacity of approximately 9166.8 liters (2421.6 gallons).

Figure 5: Side view of the original tow tank without wave making capability. In the middle of the tank on top can be seen the carriage tow plate.

A small tow carriage consisting of an aluminum plate spans the width of the tank and rides on bearings through a pair of parallel stainless steel guide rails affixed to the top of the tank. The cable driven pulley system is powered by a 3728.5 watt (five horsepower) alternating current motor, and can propeller the carriage up to a maximum speed of 9 meters per second, though typical speeds are only about 1.5 meters per second due to the constraints of the relatively short tank length. Even though the carriage is small, there is ample room for interchangeable instrumentation and sensor packages such as a data acquisition system that features a wireless router for relay of force gage data.

Wavemaker

The NPS wavemaker is based off an existing design used at the U.S. Naval Academy by the Naval Architecture and Ocean Engineering department for their sediment tank coastal wavemaker (Tran, 2016). The wavemaker, shown in Figure 6, consists of a wedge type plunger that is driven vertically into the water at one end of the tank and produces traveling waveforms down the length of the tank. The wedge is slightly less than 0.914 meters (3 feet) in width by 0.610 meters (2 feet) in depth, and was fabricated by the NPS Mechanical and Aerospace Engineering Machine Shop out of 5086 marine grade aluminum. It has a 35 degree interior angle from vertical and was welded together out of six machined sections and then marine sealant was applied to the seams. It can be seen through the Plexiglass window of the tow tank at the bottom of Figure 6. In order to generate waves, the wedge, which is cantilevered over the edge of the tank, slides up and down along the two primary vertical stations, guided through slots by Teflon roller bearings. As currently installed, the maximum vertical travel distance of the wedge is approximately 17.78 centimeters (5 inches). The two vertical guide rails and the support framing was primarily constructed out of 80/20 Inc prefabricated aluminum T-slot profiles and connectors. This system was chosen for its ease of assembly and alteration over a more traditional machined steel frame. The addition of secondary support brackets and Teflon roller guides to minimize vibrations was a minor post-installation modification to the original design.

The motion control system used to drive the wavemaker consists of a motor, controller, and linear actuator. The motor is a MOOG – Animatics MT Motor (SM34165MT) which provides a continuous torque of 1.42 N-m (12.58 in-lb) and peak torque of 3.94 N-m (34.88 in-lb) with a 133.45 Newtons (30 lbs) shaft radial load delivered through a 12.7 millimeter (0.5 in) threaded rod. It has a peak power of 1120 watts at 3330 rpm. The controller is a Modusystems Pulse/Dir controller MAC-2TC. This fixed axis count, multi-axis motion controller is interfaced through Snap2Motion software. This "drag-drop-edit" style software is based on MIT Media Labs "Scratch" software and facilitates the interactive programming and real time operation of the motion control device by students without extensive time devoted to specific code generation. Finally, the linear actuator is an E-Drive L-TAC LS long stroke ball

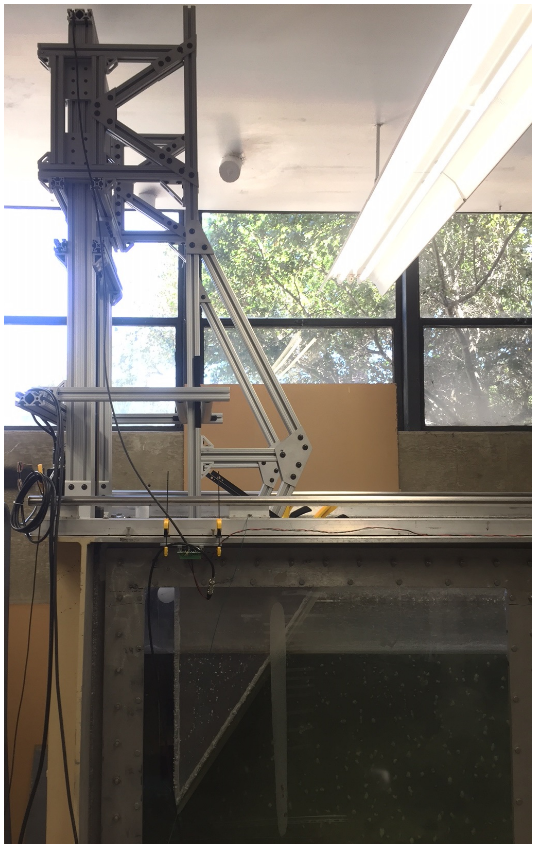

Figure 6: Side view of the wavemaker system. Attached to the top of the tank are the two vertical rails and the moving support frame. Visible in the Plexiglass side window of the tank is the aluminum wedge.

screw linear actuator (LS204-24). It has a maximum 60.96 centimeters (24 in) stroke, and can provide up to 1779.3 Newtons (400 lb) thrust, at a 40.64 centimeters per second (16 in/s) maximum velocity. A Senix ToughSonic ultrasonic probe is attached to the top frame of the wavemaker and is focused onto a portion of the oscillating frame. This allows the direct measurement of the wedge motion.

The motion of the wedge is prescribed through the superposition of up to 50 regular sine waves, each with a given amplitude, frequency, and phase, that the user inputs through the software. From such flexibility, a wide range of wave conditions ranging from simple single regular waves or pairs of regular waves all the way to traditional irregular seaways, such as JONSWAP, Bretschneider, and Pierson-Moskowitz, can be generated fairly accurately by discretizing the spectrum data from analytic relationships or even physically measured spectrum.

Due to our anticipated model size range, typical regular wave frequencies will go from 0.75 Hz to around 1.75 Hz, which corresponds to wave lengths from 2.77 meters (9.088 ft) to 0.51 meters (1.673 ft). Lower frequency, longer waves can be produced but the tank depth limits production of these waves for use in shallow water studies due to the presence of significant bottom effects. Using the current wave making setup, for sufficiently long waves, we have generated well-formed waves with maximum amplitudes of nearly 50.8 millimeters (2 inches).

Proposed Wave Absorbing Beach

The addition of wave making capabilities to the tow tank necessitates the installation of a wave absorbing beach opposite the wavemaker. The beach is necessary to minimize the presence of reflected wave energy in the tank and ensure the generated wave environment is present throughout the tank. Figure 7 shows the proposed beach and was designed by John G. Hoyt III.

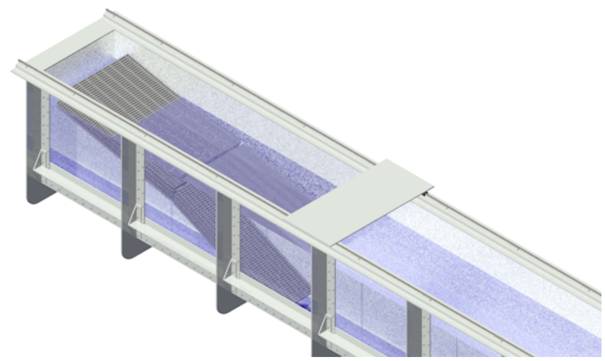

Figure 7: Proposed wave absorbing beach design (rendering courtesy of John G. Hoyt III).

The proposed beach is a two-section hinged design that allows for each section to be set at an independent angle. The design spans the width of the tank and has an approximate total length of 3.2 meters (10.5 feet). The beach consists of three layers of Seasafe GatorGrate RM1410 (HD10)-PFR material with a 2.54 by 10.16 centimeter (1” x 4”) rectangular mesh pattern. The three layers are separated vertically by fiberglass composite square tube longitudinal stiffeners. The bottom of the beach consists of solid fiberglass panels. The layers are held together with epoxy and a series of all thread rods that are attached to the top and bottom of the beach and tightened down with nylon nuts. Figure 8 shows the general lay-out of the beach.

A solid fiberglass strut channel runs along the bottom of the tank and then up the sides to create a frame. Three pairs of strut-mount routing clamp hinges slide vertically in the strut channel. A 9.525 millimeter (3/8”) diameter 316 Stainless steel rod runs between each pair of hinges and connects to the longitudinal stiffeners of the beach. By raising and lowering the hinges and rod assemblies, the elevation of the front and back of each beach section can be adjusted.

The notional beach set-up is planned to be a 12 degree upper slope and a 24 degree lower slope. However, the variability built into the design allows for the optimal pair of

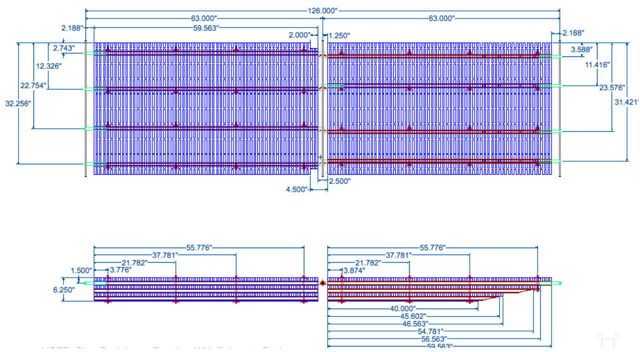

Figure 8: General lay-out of the proposed beach design (figure courtesy of John G. Hoyt III).

angles to be determined experimentally for a given wave environment and then held fixed during testing. Also, since the beach design spans all the way to the bottom of the tank, future testing of underwater vehicles in "shallow water" could be undertaken and supported by the current beach design. Finally, if needed, the beach can be dropped down to lie flat along the bottom of the tank to allow for surface ships testing in calm water to utilize the full length of the tow tank.

DESCRIPTION OF NUMERICAL FACILITY

The numerical simulation of the tow tank wave environment was done in ANSYS CFX version 17.2. ANSYS CFX, like most direct numeric simulations, discretizes the domain into a user-specified number of elements or meshes. Using an element-based finite volume method, it applies the unsteady Navier-Stokes equations to the boundaries of each element. The program time marches forward at a user-specified time step, resolving the Navier-Stokes equations at each discrete time, conserving mass, momentum, and energy.

The experimental tow tank's geometry and the wedge was duplicated within ANSYS CFX as closely as possible. Figure 9 is a side view of the geometry used by ANSYS CFX. Duplicating the overall dimensions of the tank is a straight-

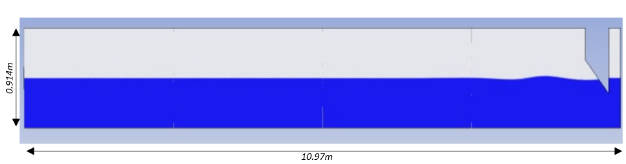

Figure 9: Geometry of the tow tank and wedge within ANSYS CFX.

forward task. The generation of the waves in the tank, however, are not made by specifying an input boundary condition. Rather, the wedge is directly forced to oscillate within the simulation to generate the waves. Further, the space behind the wedge and the small gaps on either side of the wedge are also captured in the geometry model.

The waves in the tank are generated by the fluid displaced by the wedge as it moves vertically up and down in the simulation. The wedge is an inverted right triangle with a base of 0.427 meters (1.4 feet) and a height of 0.610 meters (2 feet). This results in an angle of 35 degrees that pierces the water. Figure 10 shows the dimensions of the wedge as modeled within ANSYS CFX. The actual motion in the simulation is created by deforming the mesh at the wedge face. The vertical position of the face, z, is governed by

$$z = \left(1 - \mathrm{e}^{-3t^2}\right) a_\mathrm{w} \sin\left(2\pi f t + \phi\right) \qquad (1)$$

where a_w is the wedge amplitude, f is the oscillation frequency, and ϕ is the phase shift. The purpose of the exponential function is to capture the transitional motion from the initial rest condition to the steady-state motion of the wedge. There are numeric stability considerations that require such an initial ramp. The model controller for the actual tow tank wedge also has a transitional period as well meaning that the initial wedge motion exhibits this type of modeled behavior.

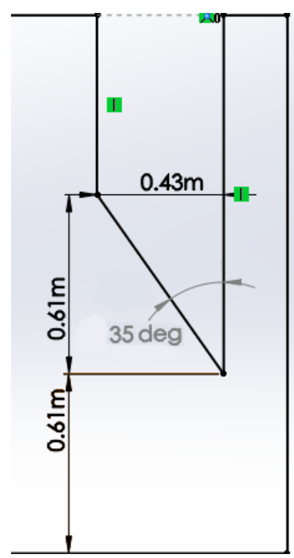

Figure 10: Dimensioned drawing of the wedge geometry used in ANSYS CFX.

The boundary conditions for the simulation were chosen to match the physical situation in the tank. The wedge face, tank bottom, and end wall were treated as no-slip boundary conditions. The top of the tank was treated as an opening allowing air to pass both directions through the boundary. Ultimately, the full width of the tank will be modeled with no-slip boundary conditions as well. But initially, only the two-dimensional centerline of the tank was simulated by making the width of the tank one element and the tank sides were treated as symmetries. The properties of the two working fluids, water and air, were based off a temperature of 25 degrees Celsius. The calm water height in the tank was 0.914m (3 feet). A K-epsilon turbulence model was applied to capture the effects of turbulence. To record wave elevation, planes were placed normal to the direction of wave propagation at 2.74 meters (9 feet), 5.49 meters (18 feet), and 8.23 meters (27 feet) from the front wall of the tank. At each time step, the water volume fraction of the elements at a particular plane of interest were summed and then divided by the tank width to calculate the average water height across the plane.

A future effort will involve modeling the proposed wave-absorbing beach directly rather then artificially extending the tank length and imposing a damping region with very high viscosity as is frequently done. Once the beach geometry is modeled, we can compare the predicted level of wave dissipation from the simulation with the actual achieved level measured in the tow tank.

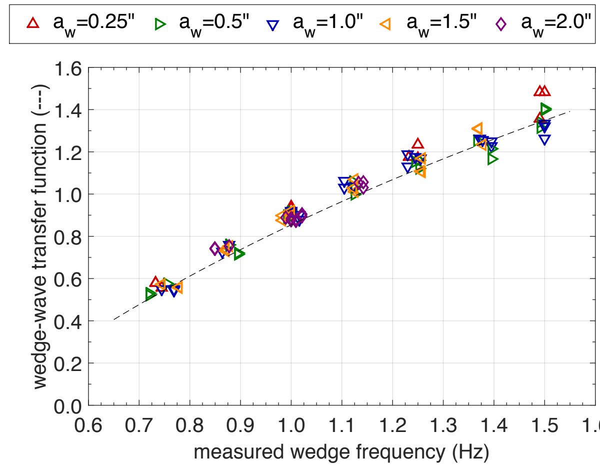

Figure 11: Wave generation transfer function for single regular wave creation. The amplitudes in the legend refer to the sinusoidal amplitude of the wedge motion.

INITIAL FINDINGS

Experimental Wave Generation

The wave generation transfer function for constant amplitude, single frequency regular waves has been experimentally measured. The transfer function, Ψ, is simply

$$\Psi = \frac{H}{2a_{\mathrm{w}}} \tag{2}$$

where H and a_{w} are the wave height and wedge amplitude respectively. A series of tests were conducted where the sinusoidal wedge motion was varied between 0.75 and 1.5 Hz and 6.35 to 50.8 millimeters (0.25 to 2.0 inches). The resultant wedge motion and wave elevation time histories were recorded. A constant amplitude, single frequency sine wave was fit to both sets of data in a least-squares sense for the steady-state middle portion of the time history. The beginning and ending transient portions were discarded. The best-fit amplitudes of the wedge motion and wave elevations are directly provided as part of the solution of the curve-fitting process. To allow for the accurate determination of the height of steep waves, the wave height was calculated using a third-order Stokes wave approximation. Therefore, the wave height, H, was estimated as

$$H = 2a\left(1+\frac{3}{8}k^2a^2\right) \tag{3}$$

where a is the wave amplitude from the sinusoidal curve-fit and k is the angular wave number $2\pi/\lambda$ with λ being the wavelength.

Figure 11 shows the experimentally determined wave-maker transfer function over the frequency range from 0.75 to 1.5 Hz. Five different wedge amplitudes, corresponding to different symbol colors, were tested. The amplitude and frequency combinations were tested more than once to provide an estimate of the uncertainty. By examining the repeatability of the results we are capturing the uncertainties due to the sensor measurement, the curve-fitting process, and the actual repeatability of the test run. The horizontal variation in the data results from the uncertainty in the actual wedge frequency estimated from the discrete Fourier transform. This uncertainty is due to the frequency resolution of the transform driven by the finite length of the time history signal.

The results of Figure 11 show that over the frequency and amplitude region tested, the transfer function is monotonically increasing and appears independent of the wedge amplitude. For wedge frequencies below roughly 1.1 Hz, the transfer function is less than unity meaning that the resultant wave amplitudes are less than the wedge amplitude. However, for wedge frequencies above 1.1 Hz, the transfer function is greater than unity and the resultant wave amplitudes are greater than the wedge amplitude.

The variation of successive waves and the amplitude dissipation as waves travel down the length of the tow tank has also been investigated. The time history of wave elevations were measured at 2.74 meters (9 feet), 5.49 meters (18 feet), and 8.23 meters (27 feet) downstream of the wedge. Figure 12 shows a representative time history of a packet of regular waves traveling down the basin and reflecting back. The particular cases shown was for a wedge oscillation frequency of 1.25 Hz and an amplitude of 19.05 millimeters (0.75 inches). The top subfigure shows the wedge motion and the quick amplitude ramp during start and stop. The time history trace also shows that the motor controller does a satisfactory job of following a single frequency, constant amplitude sine wave trajectory.

The remaining three subfigures show the measured eleva-

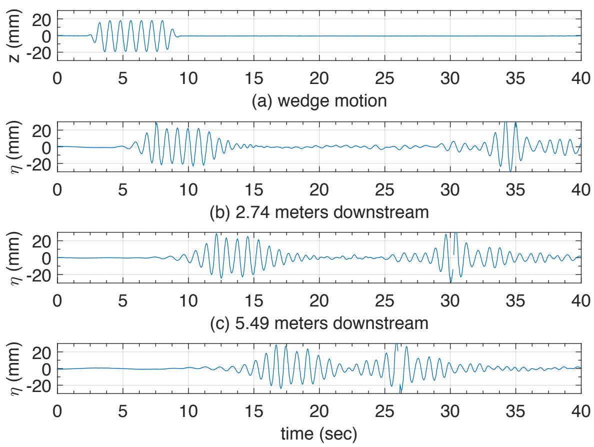

Figure 12: Wave elevation time history of a wave packet traveling the length of the tow tank and reflecting back. The top subfigure shows the wedge motion. The remaining three subfigures show the measured wave elevation at 2.74, 5.49, and 8.23 meters downstream of the wedge in the tow tank.

tion time history at 2.74, 5.49, and 8.23 meters downstream of the wedge. The probe at 2.74 meters shows a three cycle wave build up with the third cycle actually containing an overshoot. Then there are four cycles of constant amplitude corresponding to the steady oscillating portion of the wedge motion. The trailing edge of the wave packet shows the small amplitude spurious waves that resulted from stopping the wavemaker. At slightly before 35 seconds, the reflected wave is present in the data for this probe.

The probes at 5.49 and 8.23 meters show the water behavior as the wave packet moves past each of those locations. Both locations show the build-up as the wave arrives and the decay after it passes. The return of the reflected wave off the end of the tank is also clearly visible. In order to ensure accurate testing throughout the tank, it is important to ensure that waves do not get distorted as they propagate down the tank. The four constant amplitude sine waves appear to travel the majority of the length of the tank before starting to break down. As seen in the elevation data of the probe at 8.23 meters, there is no longer a set of four constant amplitude waves. Instead, it appears that low frequency waves generated during the starting and stopping of the wedge have superimposed themselves into the wave train and added a low frequency component. Considering that no beach is present, we believe that the current behavior of the tank is acceptable and once the proposed wave absorbing beach is installed and the wavemaker is run continuously, constant amplitude waves traveling the full length of the tow tank will be possible. Once the beach is installed, this will be verified experimentally.

This particular group of regular waves had an inverse steepness (λ/H) of roughly 22. The Stokes wave height modification for a wave steepness of 20 is about one percent. Therefore we expect to see the beginning of waves that are not pure sine waves but instead contain a zero mean with steeper peaks and shallower troughs. Figure 13 shows a detailed view of the constant amplitude packet of waves at 2.74 meters. In the figure, the blue 'x' data markers represent the experimentally measured data. The red line is the least-squares curve-fit of a third-order Stokes wave to the data. The fact that the red line almost perfectly fits the data confirms that the steep experimental waves had the characteristics of Stokes waves.

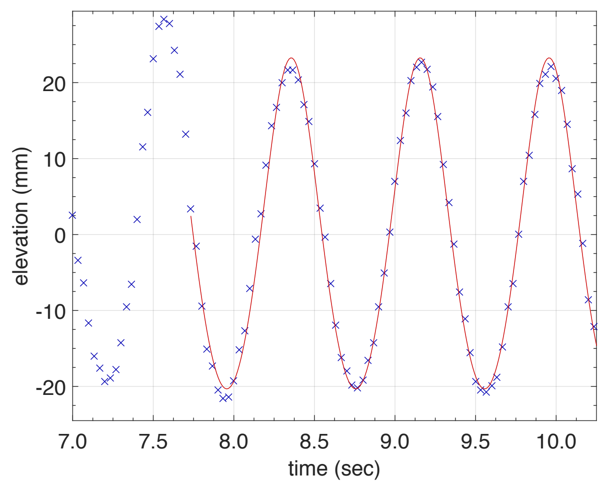

Figure 13: Detailed view of the wave packet elevation at 2.74 meters downstream. The 'x' markers denote the experimentally measured data while the red line is the least-squares curve-fit of a third-order Stokes wave.

The uniformity of the wave crests were also investigated. The 2.74 meter wave measurement location actually had three ultrasonic probes. One probe was located at the centerline of the tank, 45.72 centimeters (18 inches) from the side wall, with a second and third probe located roughly 25.4 centimeters (10 inches) and 5.08 centimetersm (2 inches) from the side wall. If the wave front was uniform, then all three measured waves should be completely in phase with each other. If, on the other hand, the wave crest was bowed, then the waves would be out of phase. Besides being able to estimate the wave amplitude from the least-squares fit of the data to a sine wave, we are also able to estimate the relative phase angle of the wave. In our case we choose to reference it relative to the sine function. The difference between the estimated relative phase angle from the centerline probe and the two probes near the wall should give a quantitative measure of the straightness of the wave crest.

Figure 14 shows the relative phase angle difference for a series of varying amplitude and frequency runs. For frequencies below 1.375 Hz, all but one run had a phase difference of less than five degrees. In many cases the difference appears to be less than 2.5 degrees. For a frequency of 1.5

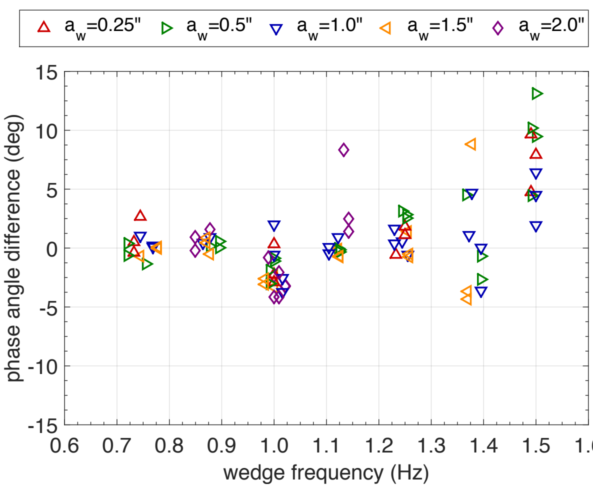

Figure 14: Relative phase angle difference of the wave elevation time histories between probes at 25.40 and 5.08 cm from the side wall of the tank and the centerline probe.

Hz, the relative phase angle difference is significantly larger. This implies that the wave crests at this high frequency begin to bow slightly. The gap between the wedge and the side of the tank is one potential cause of this. However, for frequencies below 1.375 Hz, the relative phase angle differences confirm the wedge is able to produce uniform wave fronts across the full width of the tank.

Numerical Wave Generation

Simulations were performed in the previously discussed two-dimensional numeric model. This was done by keeping the simulated wave tank 20 millimeters wide and treating the sides as symmetries. These faces have zero shear stress (free slip boundary condition) and effectively simulate an infinite domain on the other side of the boundary. Simulations were kept two-dimensional for computational efficiency since a single desktop computer with 32 processors is currently being used to run the simulations.

In the current simulations, the mesh was refined near the free surface water and air interface to a size of 5 millimeters. This element size results in approximately 5 million tetrahedral shaped elements (1 million nodes) in the mesh. Simulations performed with a coarser interface mesh than this showed unacceptable wave dissipation. In fact, the artificial dissipation was large enough that the waves had been damped out before even reaching the end of the tank. The simulation time step size was 0.01 seconds, and simulations were run for a total of 40 seconds to both ensure steady state wave generation and allow reflected wave to travel back through the tank.

Simulations without a beach or dissipation factor at the end of the tow tank were performed to study ANSYS CFX's ability to correctly simulate the wave generation process and the reflected wave behavior. The wedge in the simulation generated four complete full-amplitude oscillations, then returned to rest at the mean position of zero amplitude to match the experimental motion. The resultant wave elevations of the pulse of waves was calculated at the three different planes of interest along the tank to study and compare dissipation and reflection effects over time.

Results of both experimentally measured and numerically generated waves are shown for the case with a wedge oscillation amplitude of 50.8 millimeters (2 inches) and frequency of 1 Hz. In order to accurately access the performance of ANSYS CFX, we need to ensure that the prescribed wedge input motion is as close as possible to the actual wedge motion in the physical tow tank. Figure 15 is a comparison between the measured wave motion during the experiment (blue) and the input motion prescribed during the simulation (red). As seen in the figure, frequency and steady-state amplitude are matched very closely. There is a slight discrepancy in the rapid growth of the amplitude, with the simulation not increasing the amplitude at start-up quite enough.

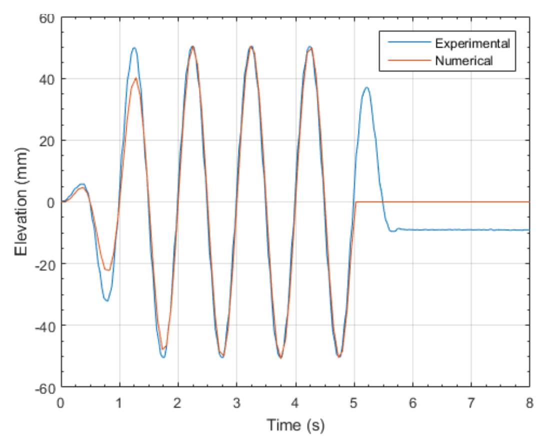

Figure 15: Comparison of experimentally measured and numerically generated wedge motions.

Figure 16 shows the comparison of wave elevation between the numeric simulation and experiment for the three probe locations of interest. The frequency of the numerically simulated waves are identical to the frequency of the experimental waves. The numerically generated waves, however, have a lower amplitude than the experimental waves. Our current theory is that this is due to an insufficiently refined mesh near the fluid interface. Our previous coarser meshes caused significant dissipation of waves as they propagated down the tank. Therefore we know that for a given input condition, the simulated wave amplitude increases with finer meshes. There exists a limit where the grid is sufficiently refined a further refinement does not produce a further increase in amplitude. We do not believe we are at that limit yet. A study is currently underway to determine the grid resolution limit. Once this is known, an

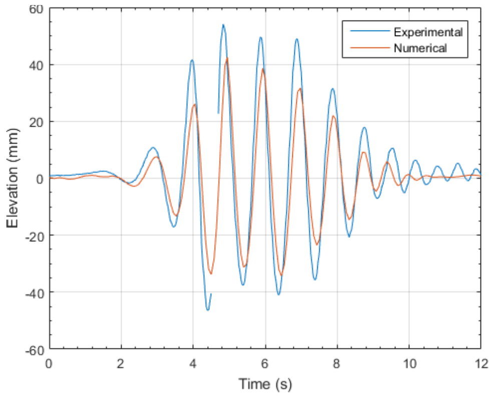

(a) 2.74 meters downstream

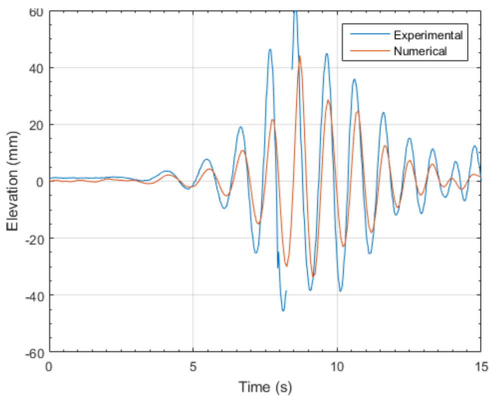

(b) 5.49 meters downstream

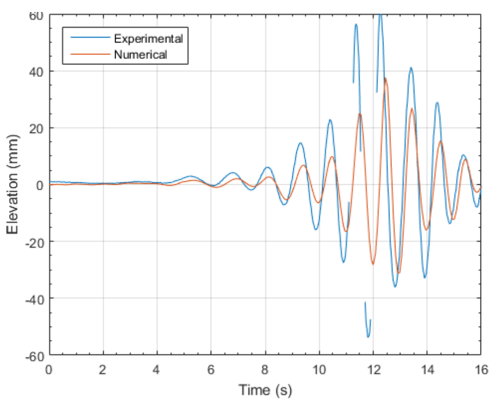

(c) 8.23 meters downstream

Figure 16: Comparison of the experimentally measured and numerically simulated wave elevation time histories at three different downstream locations.

optimal mesh size for numerically simulated surface gravity waves can be implemented which balances accuracy with feasible computational times.

Even though the amplitudes are under predicted in the simulations, there are some interesting features that are still captured. In both the experiment and the numeric simulations, the waves exhibit Stokes waves behavior. This is consistent with the behavior of steep surface gravity waves. These waves have an inverse steepness of 17 so a Stokes wave shape is expected. Stokes waves are asymmetric about the calm water line with higher crests and flatter troughs. Another interesting feature that the simulation captures is the amplitude overshoot that occurs during the initial wave build-up. In both the experimental and numerical results, as a wave packet propagates through a point along the tank, there is a steady build up in wave amplitude until the constant amplitude wave packet appears. Right before that packet appears, the preceding wave has an amplitude that is 10 to 15 percent higher.

ACKNOWLEDGMENTS

The authors wish to acknowledge the contribution of ENS Ryan Tran who worked on the wavemaker as part of his Master's thesis. ENS Tran adapted the existing U.S. Naval Academy wavemaker design to the NPS tow tank and selected the motor, linear actuator, and controller. He also procured the required materials and equipment and had the necessary machining performed.

The Research and Sponsored Programs Office at the Naval Postgraduate School provided funding for this effort as part of the institutionally funded Research Initiation Program for new faculty members (J.T. Klamo). The Consortium for Robotics and Unmanned Systems Education and Research (CRUSER) also provided funding for the current research (J.T. Klamo and Y.W. Kwon).

The views expressed in this document are those of the authors and do not reflect the official policy or position of the Department of Defense or the U.S. Government.

REFERENCES

Bryan, G. T., Platzer, M. F., & Kwon, Y. W. (2013). Experimental and computational investigation of the drag of a towed hydropower turbine. In *Proceedings of the ASME 2013 International Mechanical Engineering Congress and Exposition*. IMECE2013-63700.

Kwon, Y. W., Bolstad, S. H., Didoszak, J. M., & Rodriguez, J. A. (2016). Study of composite plate travelling in water containing ice equivalent objects. *Composite Structures*, *135*, 38–48.

Platzer, M. F., Sarigul-Klijn, N., Young, J., Ashraf, M., & Lai, J. (2011). Renewable hydrogen production using sailing ships. In *Proceedings of the ASME 2011 International Mechanical Engineering Congress and Exposition*. IMECE2011-62311.

Sarpkaya, T., & Isaacson, M. (1981). *Mechanics of wave forces on offshore structures*. (1st ed.). New York, NY: Van Nostrand Reinhold Company.

Tran, R. M. (2016). *Evaluation of composite-hull ships operating in arctic ice*. Master's thesis Naval Postgraduate School.